Genetic Algorithm–Based Optimal PWM in High Power Synchronous Machines and Regulation of Observed Modulation Error

Alireza Rezazade
Shahid Beheshti University G.C.
Arash Sayyah
University of Illinois at Urbana-Champaign
Mitra Aflaki
SAIPA Automotive Industries Research and Development Center

1. Introduction

UNIQUE features of synchronous machines like constant-speed operation, producing substantial savings by supplying reactive power to counteract lagging power factor caused by inductive loads, low inrush currents, and capabilities of designing the torque characteristics to meet the requirements of the driven load, have made them the optimal choices for a multitude of industries. Economical utilization of these machines and also increasing their efficiencies are issues that should receive significant attention. At high power rating operation, where high switching efficiency in the drive circuits is of utmost importance, optimal PWM is the logical feeding scheme. That is, an optimal value for each switching instant in the PWM waveforms is determined so that the desired fundamental output is generated and the predefined objective function is optimized (Holtz , 1992). Application of optimal PWM decreases overheating in machine and results in diminution of torque pulsation. Overheating resulted from internal losses, is a major factor in rating of machine. Moreover, setting up an appropriate cooling method is a particularly serious issue, increasing in intricacy with machine size. Also, from the view point of torque pulsation, which is mainly affected by the presence of low-order harmonics, will tend to cause jitter in the machine speed. The speed jitter may be aggravated if the pulsing torque frequency is low, or if the system mechanical inertia is small. The pulsing torque frequency may be near the mechanical resonance of the drive system, and these results in severe shaft vibration, causing fatigue, wearing of gear teeth and unsatisfactory performance in the feedback control system.

 Amongst various approaches for achieving optimal PWM, harmonic elimination method is predominant (Mohan et al., 2003), (Chiasson et al., 2004), (Sayyah et al., 2006), (Sun et al., 1996), (Enjeti et al., 1990). One of the disadvantages associated with this method originates from this fact that as the total energy of the PWM waveform is constant, elimination of low-order harmonics substantially boosts remaining ones. Since copper losses are fundamentally

determined by current harmonics, defining a performance index related to undesirable effects of the harmonics is of the essence in lieu of focusing on specific harmonics (Bose BK, 2002). Herein, the total harmonic current distortion (THCD) is the objective function for minimization of machine losses. The fundamental frequency is necessarily considered constant in this case, in order to define a sensible optimization problem (i.e. "Pulse width modulation for Holtz, J. 1996").

In this chapter, we have strove to propose an appropriate current harmonic model for high power synchronous motors by thorough inspecting the main structure of the machine (i.e. "The representation of Holtz, J 1995"), (Rezazade et al.,2006), (Fitzgerald et al., 1983), (Boldea & Nasar, 1992). Possessing asymmetrical structure in direct axis (d- axis) and quadrature axis (q-axis) makes a great difference in modelling of these motors relative to induction ones. The proposed model includes some internal parameters which are not part of machines characteristics. On the other hand, machines d and q axes inductances are designed so as to operate near saturation knee of magnetization curve. A slight change in operating point may result in large changes in these inductances. In addition, some factors like aging and temperature rise can influence the harmonic model parameters.

Based on gathered input and output data at a specific operating point, these internal parameters are determined using online identification methods (Åström & Wittenmark, 1994), (Ljung & Söderström, 1983). In light of the identified parameters, the problem has been redrafted as an optimization task, and optimal pulse patterns are sought through genetic algorithm (GA) (Goldberg, 1989), (Michalewicz, 1989), (Fogel, 1995), (Davis, 1991), (Bäck, 1996), (Deb, 2001), (Liu, 2002). Indeed, the complexity and nonlinearity of the proposed objective function increases the probability of trapping the conventional optimization methods in suboptimal solutions. The GA provided with salient features can effectively cope with shortcomings of the deterministic optimization methods, particularly when decision variables increase. The advantages of this optimization are so remarkable considering the total power of the system. Optimal PWM waveforms are accomplished up to 12 switches (per quarter period of PWM waveform), in which for more than this number of switching angles, space vector PWM (SVPWM) method, is preferred to optimal PWM approach. During real-time operation, the required fundamental amplitude is used for addressing the corresponding switching angles, which are stored in a read-only memory (ROM) and served as a look-up table for controlling the inverter.

Optimal PWM waveforms are determined for steady state conditions. Presence of step changes in trajectories of optimal pulse patterns results in severe over currents which in turn have detrimental effects on a high-performance drive system. Without losing the feed forward structure of PWM fed inverters, considerable efforts should have gone to mitigate the undesired transient conditions in load currents. The inherent complexity of synchronous machines transient behaviour can be appreciated by an accurate representation of significant circuits when transient conditions occur. Several studies have been done for fast current tracking control in induction motors (Holtz & Beyer, 1991), (Holtz & Beyer, 1994), (Holtz & Beyer, 1993), (Holtz & Beyer, 1995). In these studies, the total leakage inductance is used as current harmonic model for induction motors. As mentioned earlier, due to asymmetrical structure in d and q axes conditions in synchronous motors, derivation of an appropriate current harmonic model for dealing with transient conditions seems indispensable which is covered in this chapter. The effectiveness of the proposed method for fast tracking control has been corroborated by establishing an experimental setup, where a

field excited synchronous motor in the range of 80 kW drives an induction generator as the load. Rapid disappearance of transients is observed.

2. Optimal Synchronous PWM for Synchronous Motors

2.1 Machine Model
Electrical machines with rotating magnetic field are modelled based upon their applications and feeding scheme. Application of these machines in variable speed electrical drives has significantly increased where feed forward PWM generation has proven its effectiveness as a proper feeding scheme. Furthermore, some simplifications and assumptions are considered in modelling of these machines, namely space harmonics of the flux linkage distribution are neglected, linear magnetic due to operation in linear portion of magnetization curve prior to experiencing saturation knee is assumed, iron losses are neglected, slot harmonics and deep bar effects are not considered. In light of mentioned assumptions, the resultant model should have the capability of addressing all circumstances in different operating conditions (i.e. steady state and transient) including mutual effects of electrical drive system components, and be valid for instant changes in voltage and current waveforms. Such a model is attainable by Space Vector theory (i.e. "On the spatial propagation of Holtz, J 1996").
Synchronous machine model equations can be written as follows:

$$\boldsymbol{u}_S^R = r_S \boldsymbol{i}_R^S + j\omega \boldsymbol{\Psi}_S^R + \frac{d\boldsymbol{\Psi}_S^R}{d\tau}, \tag{1}$$

$$0 = \boldsymbol{R}_D \boldsymbol{i}_D + \frac{d\boldsymbol{\Psi}_D}{d\tau}, \tag{2}$$

$$\boldsymbol{\Psi}_S^R = \boldsymbol{l}_S \boldsymbol{i}_R^S + \boldsymbol{\Psi}_m^R, \tag{3}$$

$$\boldsymbol{\Psi}_m^R = \boldsymbol{l}_m \left(\boldsymbol{i}_D + \boldsymbol{i}_F \right), \tag{4}$$

$$\boldsymbol{\Psi}_D = \boldsymbol{l}_D \boldsymbol{i}_D + \boldsymbol{l}_m \left(\boldsymbol{i}_S + \boldsymbol{i}_F \right), \tag{5}$$

where:

$$\boldsymbol{l}_S = \boldsymbol{l}_{lS} + \boldsymbol{l}_m = \begin{pmatrix} l_d & 0 \\ 0 & l_q \end{pmatrix}, \qquad \boldsymbol{i}_F = \begin{pmatrix} 1 \\ 0 \end{pmatrix} i_F, \tag{6}$$

$$\boldsymbol{l}_m = \begin{pmatrix} l_{md} & 0 \\ 0 & l_{mq} \end{pmatrix}, \qquad \boldsymbol{l}_D = \begin{pmatrix} l_{Dd} & 0 \\ 0 & l_{Dq} \end{pmatrix} \tag{7}$$

where l_d and l_q are inductances of the motor in d and q axes; $\boldsymbol{i}_D$ is damper winding current; $\boldsymbol{u}_S^R$ and $\boldsymbol{i}_S^R$ are stator voltage and current space vectors, respectively; l_D is the damper

inductance; l_{md} is the *d*-axis magnetization inductance; l_{mq} is the *q*-axis magnetization inductance; l_{Dq} is the d-axis damper inductance; l_{Dd} is the q-axis damper inductance; $\boldsymbol{\Psi}_m$ is the magnetization flux; $\boldsymbol{\Psi}_D$ is the damper flux; i_F is the field excitation current. Time is also normalized as $\tau = \omega t$, where ω is the angular frequency. The block diagram model of the machine is illustrated in Figure 1. With the presence of excitation current and its control loop, it is assumed that a current source is used for synchronous machine excitation; thereby excitation current dynamic is neglected. As can be observed in Figure 1, harmonic component of $\boldsymbol{i}_D$ or i_F is not negligible; accordingly harmonic component of $\boldsymbol{\Psi}_m$ should be taken into account and simplifications which are considered in induction machines for current harmonic component are not applicable herein. Therefore, utilization of synchronous machine complete model for direct observation of harmonic component of stator current $\boldsymbol{i}_h$ is indispensable. This issue is subjected to this chapter.
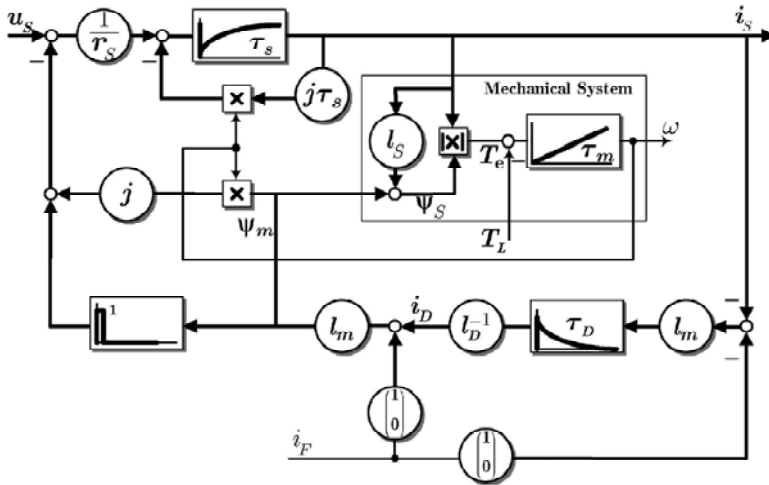

Fig. 1. Schematic block diagram of electromechanical system of synchronous machine.

2.2 Waveform Representation

For the scope of this chapter, a PWM waveform is a 2π periodic function $f(\theta)$ with two distinct normalized levels of -1, +1 for $0 \le \theta \le \pi/2$ and has the symmetries $f(\theta) = f(\pi - \theta)$ and $f(\theta) = -f(2\pi - \theta)$. A normalized PWM waveform is shown in Figure 2.
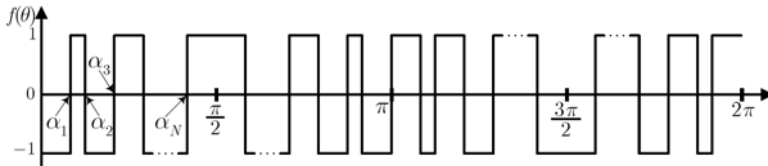
Fig. 2. One Line-to-Neutral PWM structure.

Owing to the symmetries in PWM waveform of Figure 2, only the odd harmonics exist. As such, $f(\theta)$ can be written with the Fourier series as

$$f(\theta) = \sum_{k=1,3,5,\dots} u_k \sin(k\theta) \tag{8}$$

with

$$
\begin{aligned}
u_k &= \frac{4}{\pi} \int_0^{\frac{\pi}{2}} f(\theta)\sin(k\theta) \\
&= \frac{4}{k\pi}\left(-1 + 2\sum_{i=1}^{N}(-1)^{i-1}\cos(k\alpha_i)\right).
\end{aligned}
\tag{9}
$$

2.3 THCD Formulation

The total harmonic current distortion is defined as follows:

$$\sigma_i = \sqrt{\frac{1}{T}\int_T \left[\boldsymbol{i}_S(t) - \boldsymbol{i}_{S1}(t)\right]^2 dt}, \tag{10}$$

where $\boldsymbol{i}_{S1}$ is the fundamental component of stator current.

Assuming that the steady state operation of machine makes a constant exciting current, the dampers current in the system can be neglected. Therefore, the equation of the machine model in rotor coordinates can be written as:

$$\boldsymbol{u}_S^R = \boldsymbol{r}_S \boldsymbol{i}_S^R + j\omega \boldsymbol{l}_S \boldsymbol{i}_S^R + j\omega \boldsymbol{l}_m \boldsymbol{i}_F + \boldsymbol{l}_S \frac{d\boldsymbol{i}_S^R}{d\tau} \tag{11}$$

With the Park transformation, the equation of the machine model in stator coordinates (the so called α-β coordinates) can be written as:

$$
\begin{aligned}
\boldsymbol{u}_{\alpha\beta} &= R_S \boldsymbol{i}_{\alpha\beta} + \omega(l_d - l_q)\begin{pmatrix} -\sin 2\theta & \cos 2\theta \\ \cos 2\theta & \sin 2\theta \end{pmatrix}\boldsymbol{i}_{\alpha\beta} + \frac{l_d + l_q}{2}\frac{d\boldsymbol{i}_{\alpha\beta}}{d\tau} \\
&\quad + \frac{l_d - l_q}{2}\begin{pmatrix} \cos 2\theta & \sin 2\theta \\ \sin 2\theta & -\cos 2\theta \end{pmatrix}\frac{d\boldsymbol{i}_{\alpha\beta}}{d\tau} + \omega l_{md}\begin{pmatrix} -\sin\theta \\ \cos\theta \end{pmatrix}i_F,
\end{aligned}
\tag{12}
$$

where θ is the rotor angle. Neglecting the ohmic terms in (12), we have:

$$\boldsymbol{u}_{\alpha\beta} = \frac{d}{d\tau}\left\{\boldsymbol{l}_S\left(\theta\right)\boldsymbol{i}_{\alpha\beta}\right\} + l_{md}\frac{d}{d\tau}\left\{\begin{pmatrix}\cos\theta \\ \sin\theta\end{pmatrix}i_F\right\}, \tag{13}$$

where:

$$\boldsymbol{l}_S\left(\theta\right) = \frac{l_d + l_q}{2}\boldsymbol{I}_2 + \frac{l_d - l_q}{2}\begin{pmatrix}\cos 2\theta & \sin 2\theta \\ \sin 2\theta & -\cos 2\theta\end{pmatrix}. \tag{14}$$

I_2 is the 2×2 identity matrix. Hence:

$$\boldsymbol{i}_{\alpha\beta} = \boldsymbol{l}_S^{-1}\left(\theta\right).\left\{\int\boldsymbol{u}_{\alpha\beta}d\tau - l_{md}\begin{pmatrix}\cos\theta \\ \sin\theta\end{pmatrix}i_F\right\} =$$

$$\begin{pmatrix}\dfrac{l_d + l_q}{2l_dl_q} - \dfrac{l_d - l_q}{2l_dl_q}\cos 2\theta & -\dfrac{l_d - l_q}{2l_dl_q}\sin 2\theta \\[2mm] -\dfrac{l_d - l_q}{2l_dl_q}\sin 2\theta & \dfrac{l_d + l_q}{2l_dl_q} + \dfrac{l_d - l_q}{2l_dl_q}\cos 2\theta\end{pmatrix}.\left\{\int\boldsymbol{u}_{\alpha\beta}d\tau - l_{md}\begin{pmatrix}\cos\theta \\ \sin\theta\end{pmatrix}i_F\right\} \tag{15}$$

$$= \left\{\frac{l_d + l_q}{2l_dl_q}\boldsymbol{I}_2 - \frac{l_d - l_q}{2l_dl_q}\begin{pmatrix}\cos 2\theta & \sin 2\theta \\ \sin 2\theta & -\cos 2\theta\end{pmatrix}\right\}.\left\{\int\boldsymbol{u}_{\alpha\beta}d\tau - l_{md}\begin{pmatrix}\cos\theta \\ \sin\theta\end{pmatrix}i_F\right\}$$

With further simplification, we have $i_{\alpha\beta}$ can be written as:

$$\boldsymbol{i}_{\alpha\beta} = \frac{l_d + l_q}{2l_dl_q}\int\boldsymbol{u}_{\alpha\beta}d\tau - \underbrace{l_{md}\frac{l_d + l_q}{2l_dl_q}\begin{pmatrix}\cos\theta \\ \sin\theta\end{pmatrix}i_F + l_{md}\frac{l_d - l_q}{2l_dl_q}\begin{pmatrix}\cos 2\theta & \sin 2\theta \\ \sin 2\theta & -\cos 2\theta\end{pmatrix}.\begin{pmatrix}\cos\theta \\ \sin\theta\end{pmatrix}}_{J_1}$$

$$-\frac{l_d - l_q}{2l_dl_q}\underbrace{\begin{pmatrix}\cos 2\theta & \sin 2\theta \\ \sin 2\theta & -\cos 2\theta\end{pmatrix}\int\boldsymbol{u}_{\alpha\beta}d\tau}_{J_2}. \tag{16}$$

Using the trigonometric identities, $\cos\left(\theta_1 - \theta_2\right) = \cos\theta_1\cos\theta_2 + \sin\theta_1\sin\theta_2$ and $\sin\left(\theta_1 - \theta_2\right) = \sin\theta_1\cos\theta_2 - \cos\theta_1\sin\theta_2$ the term J_1 in Equation (16) can be simplified as:

$$
\begin{aligned}
J_1 &= -l_{md}\frac{l_d+l_q}{2l_dl_q}\begin{pmatrix}\cos\theta\\\sin\theta\end{pmatrix}i_F + l_{md}\frac{l_d-l_q}{2l_dl_q}\begin{pmatrix}\cos 2\theta.\cos\theta+\sin 2\theta.\sin\theta\\\sin 2\theta.\cos\theta-\cos 2\theta.\cos\theta\end{pmatrix}i_F\\
&= -l_{md}\frac{l_d+l_q}{2l_dl_q}\begin{pmatrix}\cos\theta\\\sin\theta\end{pmatrix}i_F + l_{md}\frac{l_d-l_q}{2l_dl_q}\begin{pmatrix}\cos\theta\\\sin\theta\end{pmatrix}i_F\\
&= \frac{l_{md}}{l_d}\begin{pmatrix}\cos\theta\\\sin\theta\end{pmatrix}i_F.
\end{aligned}
\tag{17}
$$

On the other hand, writing the phase voltages in Fourier series:

$$
u_A = \sum_{s\in S_3}u_{2s+1}\sin\big((2s+1)\theta\big),\qquad u_B = \sum_{s\in S_3}u_{2s+1}\sin\left((2s+1)\left(\theta-\frac{2\pi}{3}\right)\right) \quad\text{and}
$$

$$
u_C = \sum_{s\in S_3}u_{2s+1}\sin\left((2s+1)\left(\theta-\frac{4\pi}{3}\right)\right);\quad \text{then using 3-phase to 2-phase}
$$

transformation, we have:

$$
\begin{pmatrix}u_\alpha\\u_\beta\end{pmatrix} = \begin{pmatrix}u_A\\\dfrac{1}{\sqrt{3}}(u_B-u_C)\end{pmatrix} = \begin{pmatrix}\displaystyle\sum_{s\in S_3}u_s\sin(s\theta)\\[2mm]\displaystyle\sum_{s\in S_3}u_s\sin\left(s\left(\theta-\frac{2\pi}{3}\right)+\varphi_s\right)\end{pmatrix}
\tag{18}
$$

in which:

$$
\varphi_s = \begin{cases}\dfrac{\pi}{6} & for\quad s=1,7,13,\ldots\\[3mm] -\dfrac{\pi}{6} & for\quad s=5,11,17,\ldots\end{cases}
\tag{19}
$$

As such, we have:

$$
\boldsymbol{u}_{\alpha\beta} = \begin{pmatrix}\displaystyle\sum_{l=0}^{\infty}\Big[u_{6l+1}\sin\big((6l+1)\theta\big)+u_{6l+5}\sin\big((6l+5)\theta\big)\Big]\\[3mm]\displaystyle\sum_{l=0}^{\infty}\left[u_{6l+1}\sin\left((6l+1)\left(\theta-\frac{2\pi}{3}\right)+\frac{\pi}{6}\right)+u_{6l+5}\sin\left((6l+5)\left(\theta-\frac{2\pi}{3}\right)-\frac{\pi}{6}\right)\right]\end{pmatrix}.
\tag{20}
$$

Integration of $u_{\alpha\beta}$ yields:

$$\int \boldsymbol{u}_{\alpha\beta} d\tau = -\frac{1}{\omega} \left(\begin{array}{c} \sum_{l=0}^{\infty} \left[\dfrac{u_{6l+1}}{6l+1} \cos\big((6l+1)\theta\big) + \dfrac{u_{6l+5}}{6l+5} \cos\big((6l+5)\theta\big) \right] \\ \sum_{l=0}^{\infty} \left[\dfrac{u_{6l+1}}{6l+1} \cos\left((6l+1)\theta - 4\pi l - \dfrac{\pi}{2}\right) + \dfrac{u_{6l+5}}{6l+5} \cos\left((6l+5)\theta - 4\pi l - \dfrac{3\pi}{2}\right) \right] \end{array} \right).$$

$$= -\frac{1}{\omega} \left(\begin{array}{c} \sum_{l=0}^{\infty} \left[\dfrac{u_{6l+1}}{6l+1} \cos\big((6l+1)\theta\big) + \dfrac{u_{6l+5}}{6l+5} \cos\big((6l+5)\theta\big) \right] \\ \sum_{l=0}^{\infty} \left[\dfrac{u_{6l+1}}{6l+1} \sin\big((6l+1)\theta\big) - \dfrac{u_{6l+5}}{6l+5} \sin\big((6l+5)\theta\big) \right] \end{array} \right). \tag{21}$$

By substitution of $\int \boldsymbol{u}_{\alpha\beta} d\tau$ in Equation (16), the term J_2 can be written as:

$$J_2 = \begin{pmatrix} \cos 2\theta & \sin 2\theta \\ \sin 2\theta & -\cos 2\theta \end{pmatrix} . \int \boldsymbol{u}_{\alpha\beta} d\tau$$

$$= -\frac{1}{\omega}. \left(\begin{array}{c} \left(\sum_{l=0}^{\infty} \left[\dfrac{u_{6l+1}}{6l+1} \Big[\cos\big((6l+1)\theta\big).\cos(2\theta) + \sin\big((6l+1)\theta\big).\sin(2\theta) \Big] \right] \right) \\ \left(\sum_{l=0}^{\infty} \left[\dfrac{u_{6l+1}}{6l+1} \Big[\cos\big((6l+1)\theta\big).\sin(2\theta) - \sin\big((6l+1)\theta\big).\cos(2\theta) \Big] \right] \right) \end{array} \right). +$$

$$\left(\begin{array}{c} \sum_{l=0}^{\infty} \left[\dfrac{u_{6l+5}}{6l+5} \Big[\cos\big((6l+5)\theta\big).\cos(2\theta) - \sin\big((6l+5)\theta\big).\sin(2\theta) \Big] \right] \\ \sum_{l=0}^{\infty} \left[\dfrac{u_{6l+5}}{6l+5} \Big[\cos\big((6l+5)\theta\big).\sin(2\theta) + \sin\big((6l+5)\theta\big).\cos(2\theta) \Big] \right] \end{array} \right) \tag{22}$$

$$= -\frac{1}{\omega} \left(\begin{array}{c} \sum_{l=0}^{\infty} \left[\dfrac{u_{6l+1}}{6l+1} \cos\big((6l-1)\theta\big) + \dfrac{u_{6l+5}}{6l+5} \cos\big((6l+7)\theta\big) \right] \\ \sum_{l=0}^{\infty} \left[-\dfrac{u_{6l+1}}{6l+1} \sin\big((6l-1)\theta\big) + \dfrac{u_{6l+5}}{6l+5} \sin\big((6l+7)\theta\big) \right] \end{array} \right).$$

Considering the derived results, we can rewrite $i_A = i_\alpha$ as:

$$i_A = -\frac{l_d + l_q}{2l_d l_q \omega} \sum_{l=0}^{\infty} \left[\frac{u_{6l+1}}{6l+1} \cos\big((6l+1)\theta\big) + \frac{u_{6l+5}}{6l+5} \cos\big((6l+5)\theta\big) \right]$$

$$+ \frac{l_d - l_q}{2l_d l_q \omega} \sum_{l=0}^{\infty} \left[\frac{u_{6l+1}}{6l+1} \cos\big((6l-1)\theta\big) + \frac{u_{6l+5}}{6l+5} \cos\big((6l+7)\theta\big) \right] \tag{23}$$

$$- \frac{l_{md}}{l_d} i_F \cos\theta.$$

Using the appropriate dummy variables $l = l' + 1$ and $l = l'' - 1$, we have:

$$
\begin{aligned}
i_A = & -\frac{l_d + l_q}{2l_d l_q \omega} \left\{ \sum_{l=-1}^{\infty} \frac{u_{6l+1}}{6l+1} \cos\left((6l+5)\theta\right) + \sum_{l=1}^{\infty} \frac{u_{6l+5}}{6l+5} \cos\left((6l+5)\theta\right) \right\} \\
& + \frac{l_d - l_q}{2l_d l_q \omega} \left\{ \sum_{l'=0}^{\infty} \frac{u_{6l'+7}}{6l'+7} \cos\left((6l'+1)\theta\right) + \sum_{l''=0}^{\infty} \frac{u_{6l''-1}}{6l''-1} \cos\left((6l''+1)\theta\right) \right\} - \frac{l_{md}}{l_d} i_F \cos\theta \\
= & -\frac{l_d + l_q}{2l_d l_q \omega} \left\{ \sum_{l=0}^{\infty} \frac{u_{6l+1}}{6l+1} \cos\left((6l+1)\theta\right) + \sum_{l=0}^{\infty} \frac{u_{6l+5}}{6l+5} \cos\left((6l+5)\theta\right) \right\} \\
& + \frac{l_d - l_q}{2l_d l_q \omega} \left\{ \sum_{l=0}^{\infty} \frac{u_{6l+7}}{6l+7} \cos\left((6l+5)\theta\right) + \sum_{l=0}^{\infty} \frac{u_{6l-1}}{6l-1} \cos\left((6l+1)\theta\right) + u_1 \cos\theta \right\} - \frac{l_{md}}{l_d} i_F \cos\theta
\end{aligned} \tag{24}
$$

Thus, we have i_A as:

$$
\begin{aligned}
i_A = & -\frac{1}{2l_d l_q \omega} \left\{ \sum_{l=0}^{\infty} \left[(l_d + l_q)\frac{u_{6l+1}}{6l+1} - (l_d - l_q)\frac{u_{6l-1}}{6l-1} \right] . \cos\left((6l+1)\theta\right) \right. \\
& \left. -(l_d - l_q)u_1 \cos(\theta) + \sum_{l=0}^{\infty} \left[(l_d + l_q)\frac{u_{6l+5}}{6l+5} - (l_d - l_q)\frac{u_{6l+7}}{6l+7} \right] . \cos\left((6l+1)\theta\right) \right\} \\
& -\frac{l_{md}}{l_d} i_F \cos\theta.
\end{aligned} \tag{25}
$$

Removing the fundamental components from Equation (25), the current harmonic is introduced as:

$$
\begin{aligned}
i_{Ah} = & -\frac{1}{2l_d l_q \omega} . \left\{ \sum_{l=1}^{\infty} \left[\left\{ (l_d + l_q)\frac{u_{6l+1}}{6l+1} - (l_d - l_q)\frac{u_{6l-1}}{6l-1} \right\} . \cos\left((6l+1)\theta\right) \right] + \right. \\
& \left. \sum_{l=0}^{\infty} \left[\left\{ (l_d + l_q)\frac{u_{6l+5}}{6l+5} - (l_d - l_q)\frac{u_{6l+7}}{6l+7} \right\} . \cos\left((6l+5)\theta\right) \right] \right\} \\
= & -\frac{1}{2l_d l_q \omega} . \left\{ \sum_{l=0}^{\infty} \left[\left\{ (l_d + l_q)\frac{u_{6l+7}}{6l+7} - (l_d - l_q)\frac{u_{6l+5}}{6l+5} \right\} . \cos\left((6l+7)\theta\right) \right] + \right. \\
& \left. \sum_{l=0}^{\infty} \left[\left\{ (l_d + l_q)\frac{u_{6l+5}}{6l+5} - (l_d - l_q)\frac{u_{6l+7}}{6l+7} \right\} . \cos\left((6l+5)\theta\right) \right] \right\}.
\end{aligned} \tag{26}
$$

On the other hand, σ_l^2 can be written as:

$$\sigma_l^2 = \left(\left(l_d + l_q \right) \frac{u_{6l+7}}{6l+7} - \left(l_d - l_q \right)_q \frac{u_{6l+5}}{6l+5} \right)^2 + \left(\left(l_d + l_q \right) \frac{u_{6l+5}}{6l+5} - \left(l_d - l_q \right) \frac{u_{6l+7}}{6l+7} \right)^2$$

$$= 2 \left(l_d^2 + l_q^2 \right) \left(\frac{u_{6l+7}}{6l+7} \right)^2 + 2 \left(l_d^2 + l_q^2 \right) \left(\frac{u_{6l+5}}{6l+5} \right)^2 - 4 \left(l_d^2 - l_q^2 \right) \frac{u_{6l+5} u_{6l+7}}{\left(6l+5 \right) \left(6l+7 \right)}. \tag{27}$$

With normalization of σ_l^2; i.e. $\widetilde{\sigma}_l^2 = \dfrac{\sigma_l^2}{l_d^2 + l_q^2}$ and also the definition of the total harmonic

current distortion as $\sigma_i^2 = \sum_{l=0}^{\infty} \widetilde{\sigma}_l^2$, it can be simplified as:

$$\sigma_i^2 = \sum_{l=0}^{\infty} \left\{ \left(\frac{u_{6l+5}}{6l+5} \right)^2 + \left(\frac{u_{6l+7}}{6l+7} \right)^2 - 2 \frac{l_d^2 - l_q^2}{l_d^2 + l_q^2} \left(\frac{u_{6l+5}}{6l+5} \right) \cdot \left(\frac{u_{6l+7}}{6l+7} \right) \right\} \tag{28}$$

Considering the set $S_3 = \{5,7,11,13,...\}$ and with more simplification, σ_i in high-power synchronous machines can be explicitly expressed as:

$$\sigma_i = \sqrt{ \sum_{k \in S_3} \left(\frac{u_k}{k} \right)^2 - 2 \frac{l_d^2 - l_q^2}{l_d^2 + l_q^2} \sum_{l=1}^{\infty} \left(\frac{u_{6l-1}}{6l-1} \right) \cdot \left(\frac{u_{6l+1}}{6l+1} \right) }. \tag{29}$$

As mentioned earlier, THCD in high-power synchronous machines depends on l_d and l_q, the inductances of d and q axes, respectively. Needless to say, switching angles: $\alpha_1, \alpha_2, ..., \alpha_N$ determine the voltage harmonics in Equation (29). Hence, the optimization problem consists of identification of the l_q / l_d for the under test synchronous machine; determination of these switching angles as decision variables so that the σ_i is minimized. In addition, throughout the optimization procedure, it is desired to maintain the fundamental output voltage at a constant level: $u_1 = M$. M, the so-called the modulation index may be assumed to have any value between 0 and $4/\pi$. It can be shown that α_N is dependent on modulation index and the rest of N-1 switching angles. As such, one decision variable can be eliminated explicitly. More clearly:

Minimize $$\sigma_i^2 = \sum_{k \in S_3} \left(\frac{u_k}{k} \right)^2 - 2 \frac{1 - \left(l_q / l_d \right)^2}{1 + \left(l_q / l_d \right)^2} \sum_{l=1}^{\infty} \left(\frac{u_{6l-1}}{6l-1} \right) \cdot \left(\frac{u_{6l+1}}{6l+1} \right) \tag{30}$$

Subject to

$$0 < \alpha_1 < \alpha_2 < ... < \alpha_{N-1} < \frac{\pi}{2} \qquad \text{and}$$

$$\alpha_N = \cos^{-1}\left\{ \frac{(-1)^{N-1}}{2}\left(-2\sum_{i=1}^{N-1}(-1)^{i-1}\cos(\alpha_i) + \frac{M\pi}{4} + 1 \right) \right\} \tag{31}$$

3. Switching Scheme

Switching frequency in high-power systems, due to the use of GTOs in the inverter is limited to several hundred hertz. In this chapter, the switching frequency has been set to $f_s = 200\,Hz$. Considering the frequency of the fundamental component of PWM waveform to be variable with maximum value of 50 Hz (i.e. $f_{1\max} = 50\,Hz$), then $f_s / f_{1\max} = 4$. This condition forces a constraint on the number of switches, since:

$$\frac{f_s}{f_1} = N \tag{32}$$

On the other hand, in the machines with rotating magnetic field, in order to maintain the torque at a constant level, the fundamental frequency of the PWM should be proportional to its amplitude (modulation index is also proportional to the amplitude) (Leonhard, 2001). That is:

$$M = kf_1 = \frac{k}{N}.f_s = k.\frac{f_{1\max}}{N}.\frac{f_s}{f_{1\max}}. \tag{33}$$

Also, we have:

$$M = kf_1\big|_{f_1 = f_{1\max}} = 1 \Rightarrow k = \frac{1}{f_{1\max}}. \tag{34}$$

Considering Equations (33) and (34), the following equation is resulted:

$$\frac{f_s}{f_{1\max}} = M.N. \tag{35}$$

The value of $f_s / f_{1\max}$ is plotted versus modulation index in Figure 3.

Figure 3 shows that as the number of switching angles increases and M declines from unity, the curve moves towards the upper limit $f_s / f_{1\max}$. The curve, however, always remains under the upper limit. When N increases and reaches a large amount, optimization procedure and its accomplished results are not effective. Additionally, it does not show a significant advantage in comparison with SVPWM (space vector PWM). Based on this fact, in high power machines, the feeding scheme is a combination of optimized PWM and SVPWM.

At this juncture, feed-forward structure of PWM fed inverter is emphasized. Presence of current feedback path means that the switching frequency is dictated by the current which is the follow-on of system dynamics and load conditions. This may give rise to uncontrollable high switching frequencies that indubitably denote colossal losses. Furthermore, utilization of current feedback for PWM generation intensifies system instability and results in chaos.
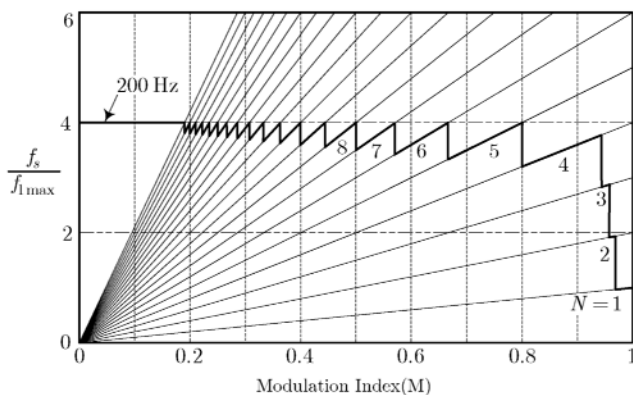
Fig. 3. Switching scheme

4. Optimization Procedure

The need for numerical optimization algorithms arises from many technical, economic, and scientific projects. This is because an analytical optimal solution is difficult to obtain even for relatively simple application problems. A numerical algorithm is expected to perform the task of global optimization of an objective function. Nevertheless, one objective function may possess numerous local optima, which could trap numerical algorithms. The possibility of failing to locate the desired global solution increases with the increase in problem dimensions. Amongst the numerical algorithms, Genetic Algorithms are one of the evolutionary computing techniques, which have been extensively used as search and optimization tools in dealing with difficult global optimization problems (Tu & Lu, 2004) that are known for the traditional optimization techniques. These traditional calculus-based optimization techniques generally require the problem to possess certain mathematical properties, such as continuity, differentiability, convexity, etc. which may not be satisfied in many real-world problems. The most significant advantage of using GA and more generally evolutionary search lies in the gain of flexibility and adaptably to the task at hand, in combination with robust performance (although this depends on the problem class) and global search characteristics (Bäck et al., 1997).
A genetic algorithm (GA) is one of evolutionary computation techniques that were first applied by (Rechenberg, 1995) and (Holland, 1992). It imitates the process of biological evolution in nature, and it is classified as one type of random search techniques. Various candidate solutions are tracked during the search procedure in the system, and the population evolves until a candidate of solution fitter than a predefined criterion emerges. In most GAs (Goldberg, 1989), a candidate solution, called an individual, is represented by a binary string, i.e., a series of 0 or 1 elements. Each binary string is converted into a phenotype that expresses the nature of an individual, which corresponds to the parameters to be determined in the problem. The GA evaluates the fitness of each phenotype. A general GA involves two major genetic operators; a crossover operator to increase the quality of individuals for the next generation, and a mutation operator to maintain diversity in the population. During the operation of a GA, individual candidate solutions are tracked in the

system as they evolve in parallel. Therefore, GA techniques provide a robust method to prevent against final results that include only locally optimized solutions. In many real-number-based techniques proposed during the past decade, it has been demonstrated that by representing physical quantities as genes, i.e., as components of an individual, it is possible to obtain faster convergence and better resolution than by use of binary or Gray coding. A program employing this kind of method is called an "Evolution Program" by (Michalewicz, 1989) or a real-coded GA. In this chapter, we adopt the real-coded GA.

The GA methodology structure for the problem considered herein is as follows:

1) Feasible individuals are generated randomly for initial population. That is a $n \times (N-1)$ random matrix, in which the rows' elements are sorted in ascending order, lying in $[0, \pi/2]$ interval.

2) Objective-function-value of all members of the population is evaluated by σ_i. This allows estimation of the probability of each individual to be selected for reproduction.

3) Selection of individuals for reproduction is done. When selection of individuals for reproduction is done, crossover and mutation are applied, based on forthcoming arguments. New population is created and this procedure continues from step (Sayyah et al.,2008). This procedure is repeated until a termination criterion is reached. Termination criteria may include the number of function evaluations, the maximum number of generations, or results exceeding certain boundaries. Other types of criteria are also possible to be defined with respect to the nature of the problem.

The crux of GA approach lies in choosing proper components; appropriate variation operators (mutation and recombination), and selection mechanisms for selecting parents and survivors, which suit the representation. The values of these parameters greatly determine whether the algorithm will find a near optimum solution and whether it will find such a solution efficiently. In the sequel, some arguments for strategies in setting the components of GA can be found.

In this chapter, deterministic control scheme as one of the three categories of parameter control techniques (Eiben et al.,1999), used to change the mutation step size, albeit rigid values considered for the rest of parameters, to avoid the problem complexity. Satisfactory results yielded in almost every stage. In the sequel, some arguments are made for strategies in setting the components of GA.

Population size plays a pivotal role in the performance of the algorithm. Large sizes of population decrease the speed of convergence, but help maintain the population diversity and therefore reduce the probability for the algorithm to trap into local optima. Small population sizes, on the contrary, may lead to premature convergences. With choosing the population size as $\lfloor (10.N)^{1.2} \rfloor$, in which the bracket $\lfloor . \rfloor$ marks that the integer part is taken, satisfying results are yielded.

Gaussian mutation step size is used with arithmetical crossover to produce offspring for the next generation. As known, a Gaussian mutation operator requires two parameters: mean value, which is often set zero, and standard deviation σ value, which can be interpreted as the mutation step size. Mutations are realized by replacing components of the vector α by

$$\alpha'_i = \alpha_i + N(0, \sigma) \qquad (36)$$

where $N(0,\sigma)$ is a random Gaussian number with mean zero and standard deviation σ. We replaced the static parameter σ by a dynamic parameter, a function σ (t) defined as

$$\sigma(t) = 1 - \frac{t}{T} \qquad (37)$$

where t, is the current generation number varying from zero to T, which is the maximum generation number.

Here, the mutation step size σ (t) will decrease slowly from one at the beginning of the run ($t = 0$) to 0 as the number of generations t approaches T. Some studies have impressively clarified, however, that much larger mutation rates, decreasing over the course of evolution, are often helpful with respect to the convergence reliability and velocity of a genetic algorithm. In this case, we have full control over the parameter and its value at time t and they are completely determined and predictable. We set the mutation probability (P_m) to a fixed value of 0.2: throughout all stages of optimization process. At first glance, choosing P_m =0.2 may look like a relatively high mutation rate. However, a closer examination reveals that the ascending order of switching angles, lying in $[0, \pi/2]$ interval, is the set of constraints in this problem. Having a relatively high mutation rate, in this problem, to maintain the population diversity, explore the search space effectively and prevent premature convergence seems completely justifiable. Notwithstanding the fact that presence of constraints significantly impacts the performance of every optimization algorithm including evolutionary computation techniques which may appear particularly apt for addressing constrained optimization problems, presence of constraints has a substantial merit which is limitation of search space and consequently decrease in computational burden and time.

Arithmetical crossover (Michalewicz, 1989) is considered herein, and probability of this operator is set to 0.8. When two parent individuals are denoted as $\alpha^k = \left(\alpha_1^{\ k}, ..., \alpha_M^{\ k}\right), k \in \{1,2\}$, two offspring $\alpha_1'^k = \left(\alpha_1'^k, ..., \alpha_M'^k\right)$ are reproduced as interpolations of both parents genes:

$$\alpha_m'^1 = \lambda \alpha_m^1 + (1-\lambda)\alpha_m^2$$
$$\alpha_m'^2 = (1-\lambda)\alpha_m^1 + \lambda \alpha_m^2 \qquad (38)$$

where λ is a constant. Tournament selection is used as the selection mechanism. It is robust and relatively simple. Tournament size is set to 2. An elitist strategy is also enabled during the replacement operation. The elitism strategy proposed by (De Jong, 1975), which has no counterpart in biology, prevents loss of a superior individual in convergence processes. It can be simply implemented by allowing the individuals with the best fitnesses in the last generation to survive into the new generation without any modifications. The purpose of this strategy is same to the purpose of the selection strategy. Elite count considered in this chapter is 3% of population size. The algorithm is repeated until a predetermined number of generations set as the general criteria for termination of algorithm, is achieved. In this chapter the termination criteria is reaching 500th generation.

4.1 Optimization Results

Accomplished optimal pulse patterns for an identified typical synchronous machine (Section V) with $l_q/l_d = 0.34$ are shown in Figure 4 based on switching scheme of Figure 3.

It should be pointed out that the insight on the distribution scheme of switching angles over the considered interval (i.e. $[0, \pi/2]$), along with tracing the increase in the number of switching angles, helped us significantly in distinguishing the suboptimal solutions from the global solution.

Corresponding total harmonic current distortion values of optimal switches are shown in Figure 5. Considering Figure 5, one point should receive a special attention. That is, although σ_i values that stand for the copper losses of motor windings decrease with reduction of the modulation index, but this descent occurs along with rise in the number switches, N. The rise in N causes switching losses in the inverter. As high-power applications are concern, switching losses should also be taken into account in feeding operation.

The optimum PWM switching angles are a function of stator voltage command, and pulse number, N. A change in voltage command due to the changes in current or speed of output controllers causes severe transients in stator currents. It should be pointed out that these changes in current or speed of controllers in a closed loop system originate from the changes in switching angles.

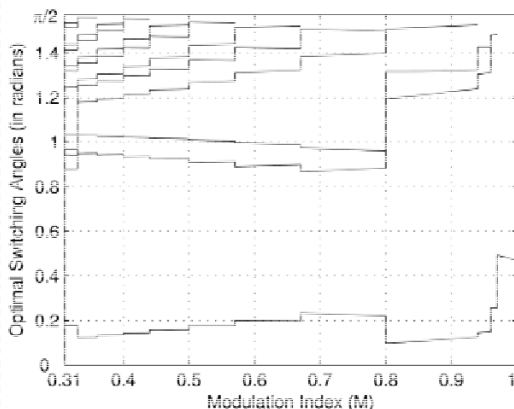The stator currents in rotor coordinates are shown in $\alpha - \beta$ plane in Figure 6.

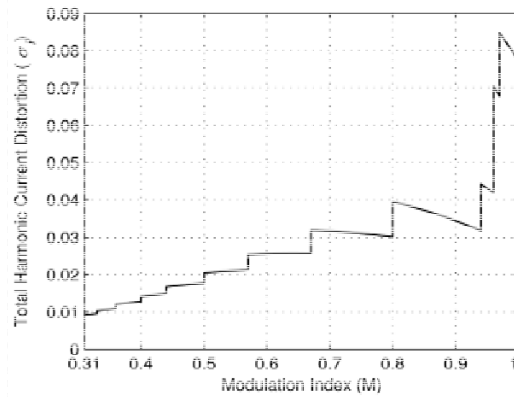Fig. 4. Optimal switching angles for $l_q/l_d = 0.34$.
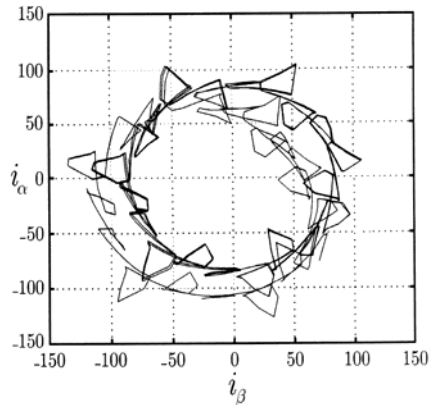
Fig. 5. Minimized total harmonic current distortion (σ_i).

Fig. 6. Over currents caused by command changes.

5. On-Line Estimation of Modulation Error

The machine currents in stator coordinates have three components:

$$
\begin{aligned}
\boldsymbol{i}_S\left(t\right) &= \boldsymbol{i}_{SS}\left(t\right) + \boldsymbol{\delta}_S\left(t\right) \\
\boldsymbol{i}_{SS}\left(t\right) &= \boldsymbol{i}_{S1}\left(t\right) + \boldsymbol{i}_{hSS}\left(t\right),
\end{aligned}
\tag{39}
$$

where $\boldsymbol{i}_{S1}\left(t\right)$ is the fundamental current component, $\boldsymbol{i}_{hSS}\left(t\right)$ is the steady state harmonic current and $\boldsymbol{\delta}_S\left(t\right)$ is the stator current dynamic modulation error and is decayed by the machine time constants (Fitzgerald et al.,1983), (Boldea & Nasar, 1992). In addition to stator dynamic modulation error, there is a field excitation modulation error that is defined as:

$$\delta_F(t) = i_F(t) - i_{F1}(t),\qquad(40)$$

which indicates its relation with transients in stator currents. For observing the modulation error and compensating it, we need better current model estimation.

5.1 Current Model Identification

Various methods have been proposed for identification of dynamical systems which are mainly classified into parametric and nonparametric approaches (Ljung L & Söderström T, 1983). In nonparametric approaches, standard inputs like step or impulse fuctions are applied, accordingly the system parameters are obtained via observation of system output. This is applicable where the knowledge of system mechanism is incomplete; offline identification is desirable; or, the properties exhibited by the system may change in an unpredictable manner. In this chapter, parametric approaches are utilized for online identification of the current harmonic model of synchronous machine and observation of modulation error. In this approach, considering the equations of synchronous machine, a model consisting of input and output in discrete form along with some coefficients as parameters has been proposed; it is tried to identify these parameters so as the outlet of the model follows the system's one. The model is then updated at each time instant in every new observation, in such a way that better convergence is achieved. The updating is performed by a recursive identification algorithm.

Unlike the asynchronous machines, in the synchronous machines, the current harmonic model is not a single total leakage inductance as established in (Holtz & Beyer, 1991), (Sun, 1995). Substitution of Equations (3) and (4) in (1) along with neglecting the dampers current yields:

$$\boldsymbol{u}_S^R = r_S \boldsymbol{i}_S^R + j\omega\left(\boldsymbol{l}_S \boldsymbol{i}_S^R + \boldsymbol{l}_m \boldsymbol{i}_F\right) + \frac{d}{d\tau}\left(\boldsymbol{l}_S \boldsymbol{i}_S^R + \boldsymbol{l}_m \boldsymbol{i}_F\right)\qquad(41)$$

After discretization of Equation (41) in T_{SS} intervals, we have:

$$\boldsymbol{u}_S^R(k) = r_S \boldsymbol{i}_S^R(k) + j\omega(k)\boldsymbol{l}_S \boldsymbol{i}_S^R(k) + j\omega(k)\boldsymbol{l}_m \boldsymbol{i}_F(k)$$
$$+\boldsymbol{l}_S \frac{\boldsymbol{i}_S^R(k+1) - \boldsymbol{i}_S^R(k)}{T_{SS}} + \boldsymbol{l}_m \frac{\boldsymbol{i}_F(k+1) - \boldsymbol{i}_F(k)}{T_{SS}}.\qquad(42)$$

with conversion of $k \rightarrow k-1$:

$$\boldsymbol{u}_S^R(k-1) = r_S \boldsymbol{i}_S^R(k-1) + j\omega(k-1)\boldsymbol{l}_S \boldsymbol{i}_S^R(k-1) + j\omega(k-1)\boldsymbol{l}_m \boldsymbol{i}_F(k-1) +$$
$$T_{SS}^{-1}\boldsymbol{l}_S \boldsymbol{i}_S^R(k) - T_{SS}^{-1}\boldsymbol{l}_S \boldsymbol{i}_S^R(k-1) + T_{SS}^{-1}\boldsymbol{l}_m \boldsymbol{i}_F(k) - T_{SS}^{-1}\boldsymbol{l}_m \boldsymbol{i}_F(k-1).\qquad(43)$$

Multiplying both sides of Equation (43) by $T_{SS}\boldsymbol{l}_S^{-1}$ and with further simplification, $\boldsymbol{i}_S^R(k)$ can be written as:

$$\boldsymbol{i}_S^R(k) = \left[\boldsymbol{I}_2 - T_{SS}\boldsymbol{l}_S^{-1}\boldsymbol{r}_S - jT_{SS}\omega(k-1)\right]\boldsymbol{i}_S^R(k-1)$$
$$+\left[\boldsymbol{l}_S^{-1}\boldsymbol{l}_m - jT_{SS}\boldsymbol{l}_S^{-1}\boldsymbol{l}_m\omega(k-1)\right]\boldsymbol{i}_F(k-1) + T_{SS}\boldsymbol{l}_S^{-1}\boldsymbol{u}_S^R(k-1) - \boldsymbol{l}_S^{-1}\boldsymbol{l}_m \boldsymbol{i}_F(k).\qquad(44)$$

Also, we have:

Thank You for previewing this eBook

You can read the full version of this eBook in different formats:

- ➢ HTML (Free /Available to everyone)

- ➢ PDF / TXT (Available to V.I.P. members. Free Standard members can access up to 5 PDF/TXT eBooks per month each month)

- ➢ Epub & Mobipocket (Exclusive to V.I.P. members)

To download this full book, simply select the format you desire below